Chemical Science

ROYAL SOCIETY OF CHEMISTRY

EDGE ARTICLE

View Article Online
View Journal | View Issue





Cite this: *Chem. Sci.*, 2024, **15**, 6800

All publication charges for this article have been paid for by the Royal Society of Chemistry

# Long-range electrostatic effects from intramolecular Lewis acid binding influence the redox properties of cobalt–porphyrin complexes†

Jose L. Alvarez-Hernandez, ‡[a] Xiaowei Zhang, ‡[b] Kai Cui, [c] Anthony P. Deziel,[a] Sharon Hammes-Schiffer, *[c] Nilay Hazari, *[a] Nicole Piekut[a] and Mingjiang Zhong *[b]

Received 20th November 2023
Accepted 2nd April 2024

DOI: 10.1039/d3sc06177a

rsc.li/chemical-science

A $Co^{II}$–porphyrin complex (**1**) with an appended aza-crown ether for Lewis acid (LA) binding was synthesized and characterized. NMR spectroscopy and electrochemistry show that cationic group I and II LAs (*i.e.*, $Li^+$, $Na^+$, $K^+$, $Ca^{2+}$, $Sr^{2+}$, and $Ba^{2+}$) bind to the aza-crown ether group of **1**. The binding constant for $Li^+$ is comparable to that observed for a free aza-crown ether. LA binding causes an anodic shift in the $Co^{II}/Co^{I}$ couple of between 10 and 40 mV and also impacts the $Co^{III}/Co^{II}$ couple. The magnitude of the anodic shift of the $Co^{II}/Co^{I}$ couple varies linearly with the strength of the LA as determined by the $pK_a$ of the corresponding metal–aqua complex, with dications giving larger shifts than monocations. The extent of the anodic shift of the $Co^{II}/Co^{I}$ couple also increases as the ionic strength of the solution decreases. This is consistent with electric field effects being responsible for the changes in the redox properties of **1** upon LA binding and provides a novel method to tune the reduction potential. Density functional theory calculations indicate that the bound LA is 5.6 to 6.8 Å away from the $Co^{II}$ ion, demonstrating that long-range electrostatic effects, which do not involve changes to the primary coordination sphere, are responsible for the variations in redox chemistry. Compound **1** was investigated as a $CO_2$ reduction electrocatalyst and shows high activity but rapid decomposition.

## Introduction

Metalloenzymes often use secondary coordination sphere effects, such as hydrogen bonding, intramolecular proton shuttles, or oriented electric fields, to achieve high activity and selectivity for a specific transformation.[1] This has inspired the design of many transition metal catalysts containing ancillary ligands that stabilize the transition state in the turnover limiting step through secondary coordination sphere effects.[2] The vast majority of these systems incorporate functional groups that promote hydrogen bonding or can act as intramolecular proton shuttles.[3] In contrast, electric field effects have not been investigated as extensively in synthetic systems.[4] This is in part because it is challenging to orient a freely diffusing molecular catalyst so that it experiences a uniform electric field.

One attractive strategy for understanding the impact of electric fields on transition metal catalysts in solution involves using an internal electrostatic field.[4c,d,f,i–l] For example, the binding of a Lewis acidic cation, such as an alkali or alkaline earth metal ion to a prepositioned site on an ancillary ligand, can alter the redox properties of a metal center due to electrostatic effects.[5] Crown or aza-crown ethers are attractive as binding sites for cationic Lewis acids (LAs) because they have high and tunable binding constants for alkali or alkaline earth metal cations.[6] Consequently, several ligands have been designed which feature pendant crown or aza-crown ether moieties, **A–E** (Fig. 1).[4l,5a,5c,d,5h,7] In many of these systems, one or two of the atoms in the crown (**A** or **B**), bind directly to the transition metal center or effect the donor properties of the ligand (**C** or **D**), making it challenging to disambiguate changes in the primary coordination sphere from electrostatic effects caused by binding of the LA cation. Further, in **A–C**, the LA is often close (~3 Å) to the transition metal, which can reduce the ability of the crown or aza-crown ether to bind the LA cation. We propose that there is value in developing systems where electrostatic effects can be tuned without significantly perturbing the electronic properties of the ligand directly bound to the transition metal, as this allows for independent control of

[a]*Department of Chemistry, Yale University, New Haven CT 06520, USA. E-mail: nilay.hazari@yale.edu*

[b]*Department of Chemical and Environmental Engineering, Yale University, New Haven CT 06520, USA. E-mail: mingjiang.zhong@yale.edu*

[c]*Department of Chemistry, Princeton University, Princeton, NJ 08544, USA. E-mail: shs566@princeton.edu*

† Electronic supplementary information (ESI) available: Additional information about selected experiments, characterizing data, NMR spectra, cyclic voltammograms, Job plots, and computational details. See DOI: https://doi.org/10.1039/d3sc06177a

‡ Authors contributed equally.

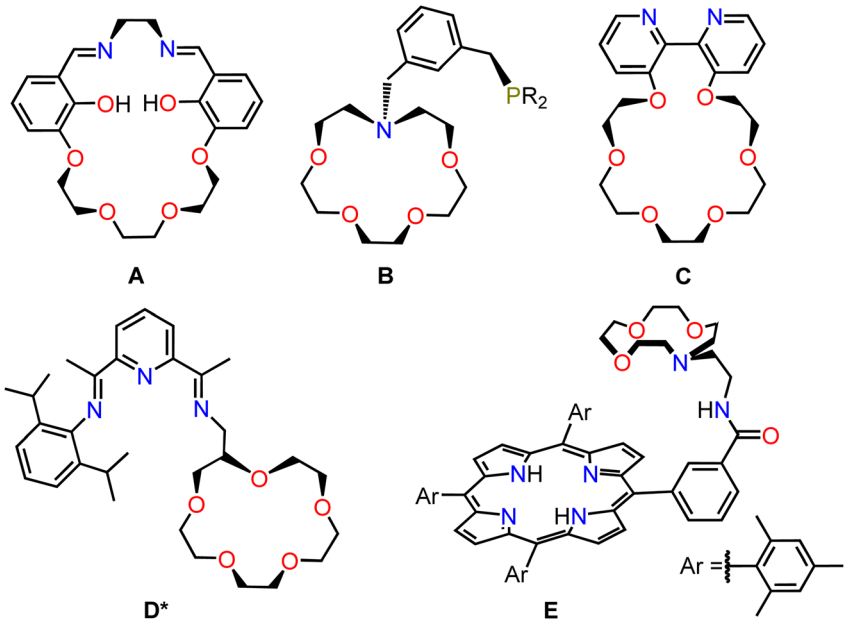


Fig. 1 Selected ligands featuring appended crown or aza-crown ether groups reported in the literature. *Ligand D was not isolated independently but was prepared *in situ* with an Fe coordinated to the pyridinediimine ligand.

primary and secondary coordination sphere effects and a high LA binding constant.

Porphyrin-ligated transition metal complexes are used as electro-, photo, and thermal catalysts for a wide variety of societally important transformations, including $CO_2$ reduction,[8] $O_2$ reduction,[8c,9] $H_2$ evolution,[9a,10] polymerization,[11] C–H functionalization,[12] epoxidation,[13] and alcohol oxidation.[14] As such, porphyrins are a privileged class of ligand and represent attractive targets for the introduction of crown ether or aza-crown ethers to explore electrostatic effects. There are reports of symmetric porphyrins containing two or four pendant crown ether groups,[15] however, this results in complexes that can bind a variable numbers of Lewis acidic cations, which complicates the interpretation of any changes in reactivity caused by LAs. Recently, Zhong *et al.* prepared a rare example of an asymmetric porphyrin ligand, **E**,[16] containing a single aza-crown ether site for LA binding, which does not directly connect to atoms in the primary coordination sphere (Fig. 1).[15f,17] We propose that this porphyrin ligand is optimal for studying internal electrostatic field effects caused by LA binding because the aza-crown ether group should be able to bind a variety of different cationic LAs and is remote from the primary coordination sphere.

In this work, we prepared a $Co^{II}$ complex (**1**, Fig. 2) supported by ligand **E**. We show that **1** can bind a variety of LAs and that the binding constant for $Li^+$ is similar to that observed for a free aza-crown ether. Further, for alkali and alkaline earth metal cations, binding to the aza-crown ether causes predictable changes to the redox properties of the Co center. Remarkably, these changes occur despite the LA being 5.6 to 6.8 Å away from the Co center, demonstrating that 'long-range' electrostatic effects can be used to tune the redox properties of the transition metal center. Finally, we demonstrate that changes in the redox properties of the Co center caused by LA binding depend on the ionic strength of the solution, which provides a handle for

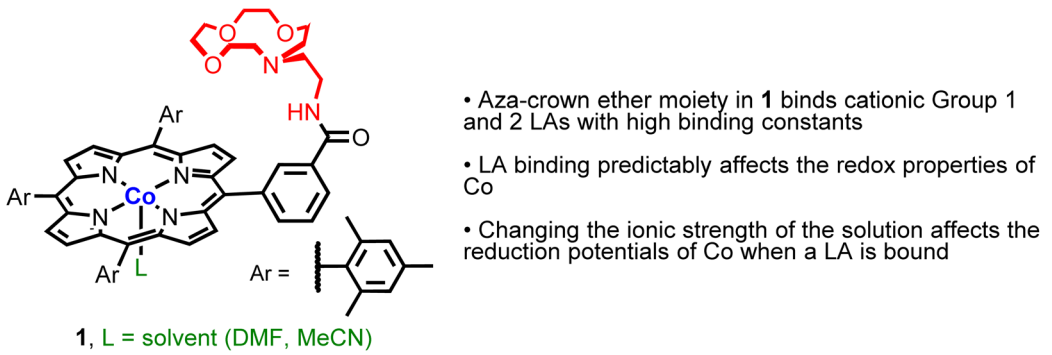


Fig. 2 Structure and properties of the new $Co^{II}$–porphyrin complex **1**, which can bind LAs, such as $Li^+$, $Na^+$, $K^+$ $Ca^{2+}$, $Ba^{2+}$, and $Sr^{2+}$, through the pendant aza-crown ether.

modulating the redox properties of Co without changing the LA or ancillary ligand structure. Overall, this work provides new insight into how to modulate induced electric fields caused by LA binding to an ancillary ligand to change the properties of a transition metal complex.

## Results and discussion

### Synthesis and characterization of cobalt–porphyrin complexes

Given that $Co^{II}$ porphyrin complexes are active catalysts for a wide variety of transformations including electrocatalytic $CO_2$ reduction,[8] we chose to react ligand **E** with $Co(OAc)_2$ to form complex **1**. The synthesis of **1** followed standard literature procedures,[18] but to ensure full metalation of the ligand a five-fold molar excess of $Co(OAc)_2$ was utilized (eqn (1)). Over the course of the reaction, two additional portions of $Co(OAc)_2$ were added to maintain an excess of $Co^{II}$ ions in solution throughout the reaction. To remove excess $Co(OAc)_2$ from **1**, our purification procedure included washing the crude reaction mixture with an aqueous solution of sodium ethylenediaminetetraacetate (EDTA), which binds tightly to free $Co^{II}$ ions in solution. As a control compound, we prepared the $Co^{II}$ complex **2**, which contains a similar porphyrin ligand to **1**, without an intramolecular LA binding site (the full synthesis and characterization data for this new ligand is provided in the SI, see Fig. S1–S3†). Both **1** and **2** were purified by column chromatography and isolated in yields of 86 and 87%, respectively.

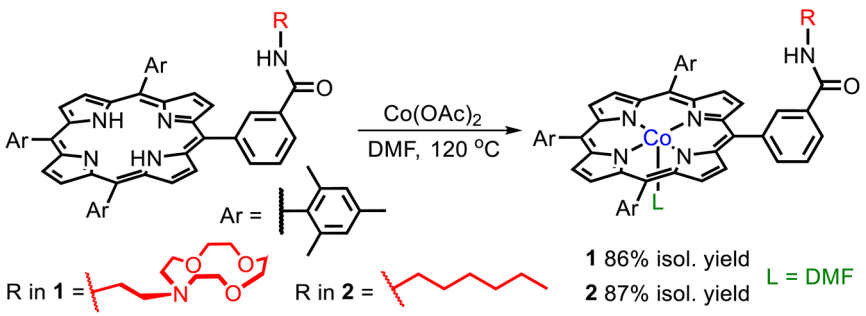


(1)

Complexes **1** and **2** were characterized using UV-vis, $^1$H NMR and EPR spectroscopy and high-resolution mass spectrometry (HRMS) (Fig. S4–S11†). The UV-vis spectrum of **1** is similar to those of other Co porphyrin complexes.[19] The spectrum is dominated by a Soret band centered at 413 nm, with a smaller Q band at 530 nm, which has a shoulder at 550 nm. These absorption bands are proposed to originate from porphyrin-centered $\pi$–$\pi^*$ electronic transitions.[20] The presence of two Q bands serves as an indicator of complete ligand metalation as free deprotonated porphyrins typically exhibit four bands in this spectral region, due to the lower symmetry of the free ligand relative to the metalloporphyrin.[20,21] Complex **1** is paramagnetic, and therefore the $^1$H NMR spectrum of **1** is complicated. In $d_8$-toluene, signals are observed between 0 and 17 ppm with the pyrrolic protons appearing the furthest downfield given their close proximity to the paramagnetic $Co^{II}$ ion. Tentative assignment of the $^1$H NMR signals is provided in the SI. EPR spectra of Co complexes are often complex, given that $^{59}$Co is the only naturally occurring isotope of Co with a nuclear spin of 7/2. The X band EPR spectrum of **1** in toluene at 7 K (Fig. 3a) displays rhombic symmetry with observable hyperfine coupling from $^{59}$Co to $g_x$, $g_y$, and $g_z$. The 8 expected peaks can be seen for $g_x$, whereas overlap of $g_y$ and $g_z$ convolute the splitting. Through simulation of the spectrum, $g$ values ($g_z$ = 2.598, $g_y$ = 2.375, and $g_x$ = 1.955) and the principal values of hyperfine interaction ($A_z$ = 330 MHz, $A_y$ = 325 MHz, $A_x$ = 360 MHz) were determined. These values are comparable to previous reports for Co tetraphenyl porphyrin complexes with axial ligands.[22] The spectroscopic data for **2** is similar to that for **1** and supports the proposed structure (Fig. S7–S10†). Unfortunately, despite repeated attempts we were unable to grow single crystals of **1** or **2** suitable for analysis using X-ray diffraction, and therefore structural information about **1** was obtained using density functional theory (DFT) calculations (*vide infra*).

Cyclic voltammograms of **1** and **2** were collected in acetonitrile (MeCN) solution under an inert atmosphere. They exhibit three clear redox events, as shown in Fig. 3b for complex **1** (see Fig. S11† for cyclic voltammograms of **2**). The first redox wave for **1** at −0.084 V *vs.* $Fc^+$/Fc (all potentials herein are reported *vs.* the ferrocenium/ferrocene, $Fc^+$/Fc, internal standard) is assigned as the $Co^{III}$/$Co^{II}$ couple based on previous literature reports.[23] This couple is quasi-reversible as changing from an octahedral $d^6$ $Co^{III}$ species to a $d^7$ $Co^{II}$ species leads to axial distortions due to Jahn–Teller effects. The large reorganization energy associated with this distortion decreases the rate of electron transfer from the electrode to **1** in solution, which impacts the reversibility of the couple. The second and third redox couples at −1.288 and −2.459 V are reversible and, based on literature precedent, are assigned as the $Co^{II}$/$Co^{I}$ couple and a ligand centered reduction.[23] Overall, the well-defined redox chemistry observed for **1** makes it ideal for studying the effects of LA binding on its redox properties. Further, the nearly

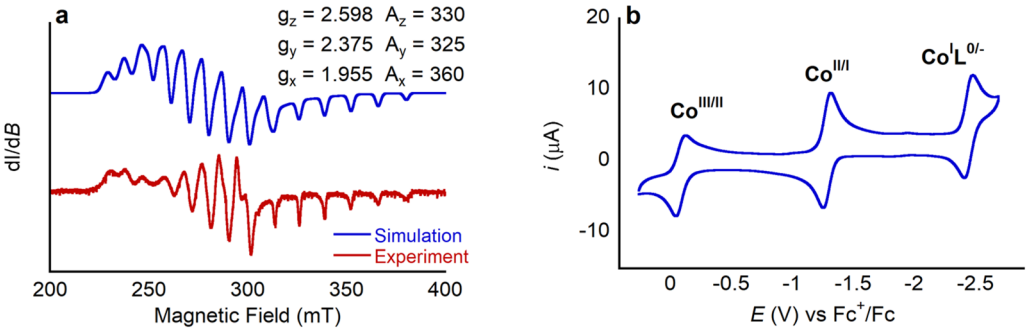


Fig. 3 (a) EPR spectrum of **1**. (b) Cyclic voltammogram of **1** (0.5 mM) in 0.25 M $TBAPF_6$ in MeCN at 100 mV $s^{-1}$ under Ar.

identical cyclic voltammograms observed for **1** and **2** indicates that the incorporation of the pendant LA binding site has negligible impact on the electronic properties of the Co center in **1**.

### Lewis acid binding to 1

To determine whether complex **1** effectively binds Lewis acidic group I and II cations, we initially performed HRMS experiments. We prepared solutions containing either **1** or **2** in MeCN and added LiOTf (OTf = triflate) or $Ca(OTf)_2$. Triflate was selected as the anion due to its non-coordinating nature and the commercial availability of a wide variety of alkali and alkali earth triflate salts. Whereas solutions of **1** showed peaks at *m*/*z* ratios consistent with the binding of $Li^+$ or $Ca^{2+}$ (Fig. S12–S15†), these peaks were absent in the HRMS of **2** (Fig. S16–S17†). This strongly suggests that **1** can bind LAs but that **2**, which lacks the pendant aza-crown ether, cannot. However, this experiment provides no information about the strength of the interaction between **1** and the LA or where binding is taking place.

To gain more quantitative information about LA binding, we used $^7$Li NMR spectroscopy to probe the binding of LiOTf to **1** and **2** in $d_3$-MeCN. We performed the experiments with a 10-fold molar excess of LiOTf relative to **1** (*vide infra*). Similar behavior was observed with 0.25 M $TBAPF_6$ electrolyte present, added to model electrochemical conditions (Fig. S18–S23†). At room temperature in the presence of 10 equivalents of LiOTf, both **1** and **2** exhibit a single peak at approximately −2.4 ppm (Fig. 4), although the peak for **1** is significantly broader than that of **2**. This is consistent with an exchange process involving rapid binding and decoordination of $Li^+$ to the aza-crown ether in **1**. At −40 °C, two distinct peaks are observed in the $^7$Li NMR spectrum for **1** in the presence of LiOTf. We assign the peak at 0.13 ppm to $Li^+$ bound to the aza-crown ether of **1**, because similar chemical shifts have been observed for $Li^+$ coordinated to crown ethers in the past,[24] and the other to free solvated $Li^+$. Presumably, at −40 °C the exchange between coordinated and solvated $Li^+$ is slow on the NMR timescale. As expected, at −40 °C, only a peak corresponding to solvated $Li^+$ is observed when **2** is cooled in the presence of LiOTf.

The observation of a single peak in the $^7$Li NMR spectra at 25 °C when LiOTf is added to **1** (Fig. 5 and S24†) is indicative of fast exchange on the NMR timescale between coordinated and solvated $Li^+$. It has been demonstrated that, in cases where there is fast exchange between free and complexed metal ions, the observed chemical shift of the resulting single NMR peak can be used to determine the binding constant ($K_b$).[24a,25] $K_b$ for a 1 : 1 $Li^+$ to **1** adduct was determined from the variation of the $^7$Li chemical shift with the increasing concentration of LiOTf relative to **1** according to a 1 : 1 general binding isotherm described by eqn (2),[25a]

$$\delta_{obs} = \frac{(\delta_{ML} - \delta_{Li})}{2C_{Li}}\left[\left(C_l + C_{Li} + \frac{1}{K_b}\right) - \sqrt{\left(C_l + C_{Li} + \frac{1}{K_b}\right)^2 - 4C_l C_{Li}}\right] + \delta_{Li} \quad (2)$$

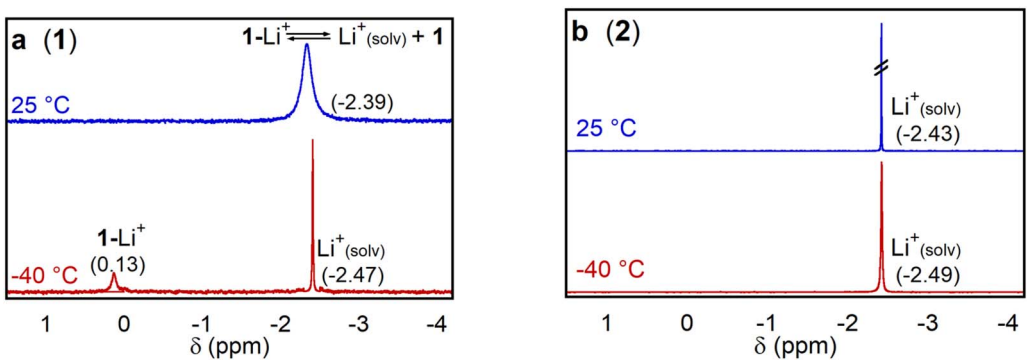


Fig. 4 $^7$Li NMR spectra of 15 mM LiOTf with 1.5 mM of (a) **1** and (b) **2** at temperatures of 25 and −40 °C in $d_3$-MeCN.

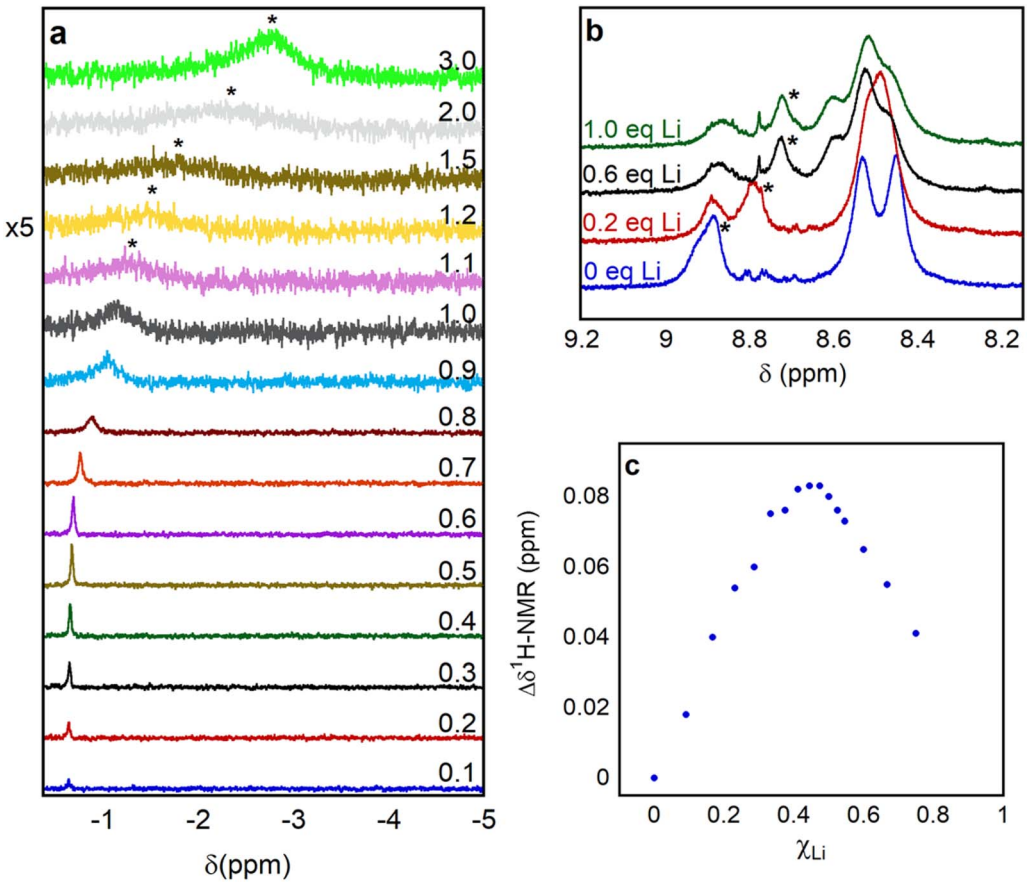


Fig. 5 Chemical shift variation in the (a) $^{7}$Li NMR and (b) $^{1}$H NMR spectra upon adding increasing amounts of LiOTf to a solution containing 1.5 mM of **1** in $d_3$-MeCN. For the $^{1}$H NMR spectra, only the peaks that proved more sensitive to added LiOTf are shown. (c) Job plot obtained from the $^{1}$H NMR peak initially centered at 8.84 ppm showing a maximum near a Li molar fraction ($\chi_{Li}$) 0.5 consistent with formation of a 1 : 1 adduct between Li and **1**.

where $\delta_{obs}$ corresponds to the measured chemical shift, $\delta_{Li}$ and $\delta_{ML}$ represent the chemical shift of the free and complexed $Li^+$ ion, respectively, and $C_{Li}$ and $C_1$ are the total concentrations of $Li^+$ and **1**. A non-linear least squares curve fitting program was used to determine $K_b$ (Fig. S27†) yielding a value of $1.2 \pm 0.3 \times 10^4$ $M^{-1}$; a similar value of $1.3 \pm 0.3 \times 10^4$ $M^{-1}$ was found when the titration was performed in the presence of 0.25 M $TBAPF_6$ (Fig. S24 and S27†) to better represent the solution composition used in our electrochemical studies (*vide infra*). Interestingly, this binding constant is similar to that of a precursor of the ligand **E**, which we also titrated with LiOTf (Fig. S28–S31†). Monitoring the addition of LiOTf to this precursor *via* $^{7}$Li NMR spectroscopy generated a $K_b$ of $2.6 \pm 0.6 \times 10^4$ $M^{-1}$ (Fig. S28–S29†), which is the same order of magnitude as previously reported $Li^+$ binding constants to free 12-crown-4 ether in MeCN.[26] This stands in contrast to other previous metal complexes featuring crown or aza-crown ether binding sites, where the affinity for alkali metals is significantly lower, up to 3 orders of magnitude, relative to the corresponding free crown.[27] We postulate that high binding affinity for the LA is important in order to ensure the LA is bound during catalytic conditions. Further, in the case of $CO_2$ reduction, strong binding of the LA cation to the crown is required to prevent the formation of insoluble carbonate salts between the Lewis acidic cation and carbonate anions formed due to $CO_2$ hydrolysis. In previous work, formation of insoluble carbonates at the working electrode has been linked to electrode fouling, causing loss of activity for molecular $CO_2$ reduction catalysts in the presence of LA salts.[28] Electrode fouling was also observed in electrochemical $CO_2$ reduction using a Re complex featuring the ligand **C** in Fig. 1, which had a low binding constant for $Li^+$ of $10^2$ $M^{-1}$.[5e] Interestingly, the precipitation of carbonate salts seen in $CO_2$ reduction catalysis by $[Mn(bpy)(CO)_3Br]$ in the presence of $Mg(OTf)_2$ (ref. 28b) was inhibited by switching the LA species to $[Zn(cyclam)]^{2+}$,[29] supporting the hypothesis that tighter binding of the LA is a viable strategy to suppress the formation of insoluble carbonates and subsequent electrode fouling.

In principle, changes in the chemical shift of peaks in the $^{1}$H NMR spectra of **1** upon the titration of a LA can be used to construct Job plots and estimate $K_b$ in an analogous fashion to $^{7}$Li NMR spectroscopy. However, analyzing $^{1}$H NMR spectra of **1** in the presence or absence of LAs is complicated by the paramagnetism of **1**. Nevertheless, we were able to identify specific peaks in the $^{1}$H NMR spectrum of **1** that move predictably upon the addition of Lewis acidic cations (Fig. 5b and S32–S35†). For example, we used the change in the chemical shift of the peak at

8.8 ppm in the presence of LAs to construct Job plots upon addition of a variable number of equivalents of LiOTf, NaOTf, and KOTf to **1** (Fig. 5c, S25, S26, and S34†). The Job plots are consistent with the formation of a 1 : 1 complex between the LA and **1**, although the quality of the data for NaOTf and KOTf is low. Unfortunately, we were unable to use eqn (1) to determine $K_b$ using the change in chemical shift in the $^1$H NMR spectra upon LA binding as poor fits were observed likely due to the presence of broad and overlapping peaks. When 0.1 equivalents of $Ca(OTf)_2$, which contains a dicationic metal ion, was added to **1**, the peak in the $^1$H NMR spectrum centered at 8.9 ppm broadens significantly more than with the monocationic LAs (Fig. S36†). If more equivalents of $Ca(OTf)_2$ are added, the peak at 8.9 ppm is not observable, presumably because it has broadened into the baseline. This suggests that for 12-$O_3$N aza-crown ether, $K_b$ is higher for $Ca^{2+}$ than for $Li^+$ and other group I cations, even though an absolute binding constant could not be determined. Consistent with this observation free 12-crown-4 is known to bind more strongly to $Ca^{2+}$ than to $Li^+$ in acetonitrile.[24b]

### Electrochemical investigation of the binding of group I and II cations to 1

To explore how LA binding impacts the redox properties of **1**, we conducted an electrochemical investigation using cyclic voltammetry. Initially, as a control, we added 30 equivalents of TBAOTf to a solution of **1** in MeCN containing 0.25 M $TBAPF_6$ as a supporting electrolyte. The cyclic voltammogram in the presence of TBAOTf was identical to the cyclic voltammogram in its absence (Fig. S37†), indicating that triflate does not interact with **1**. Cyclic voltammograms were then recorded in the presence of different amounts of $Li^+$, $Na^+$, $K^+$, $Ca^{2+}$, $Sr^{2+}$, and $Ba^{2+}$ triflate salts (Fig. 6 and S38–S42†). In each case the addition of the LA anodically shifts the position of both the $Co^{III}/Co^{II}$ and the $Co^{II}/Co^{I}$ couple, as demonstrated in Fig. 6 for one equivalent of $Ca(OTf)_2$. Addition of LA causes the ligand centered reduction at −2.459 V to become irreversible (Fig. S43†) and consequently the $Co^{II}/Co^{I}$ couple also becomes irreversible if the cyclic voltammogram window is extended to include the ligand centered reduction. This observation suggests an electrodegradation pathway in which the LA reacts with the radical-anion species formed upon reduction of the ligand. Hence, we did not extensively explore the impact of LAs on the ligand centered reduction at −2.459 V. Importantly, when LAs are added to solutions of **2**, no changes are observed by cyclic voltammetry (Fig. 6). This observation supports the hypotheses that the pendant aza-crown ether can bind LAs and that this binding is crucial to modulating the redox properties of **1**.

The magnitude of the anodic shift of the $Co^{II}/Co^{I}$ couple of **1** increases as the concentration of the LA increases, before stabilizing when a certain number of equivalents of LA are reached (Fig. 7, Tables S2 and S3†). Importantly, the reversibility of the $Co^{II}/Co^{I}$ couple is maintained regardless of the amount of LA salt present. The saturation point of the change in reduction potential is reached with a lower number of equivalents of LA for the dicationic systems compared to the monocationic systems. For example, the changes in the position of the $Co^{II}$/

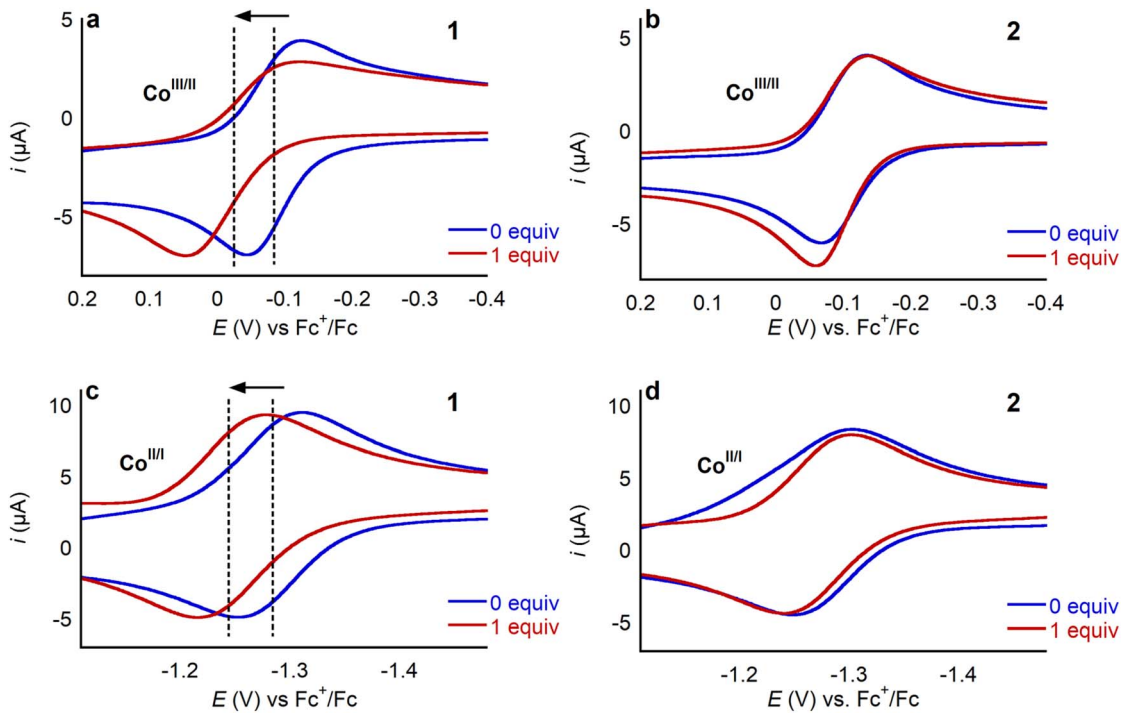


Fig. 6 Cyclic voltammograms of the $Co^{III}/Co^{II}$ (a) and (b) and $Co^{II}/Co^{I}$ (c) and (d) couples of **1** and **2**, respectively, in the absence of LA and upon addition of 1 equivalent of $Ca(OTf)_2$, showing that only for **1** does the added LA impact the CV response. Cyclic voltammograms were collected at 100 mV $s^{-1}$ in 0.25 M $TBAPF_6$ in MeCN under Ar.

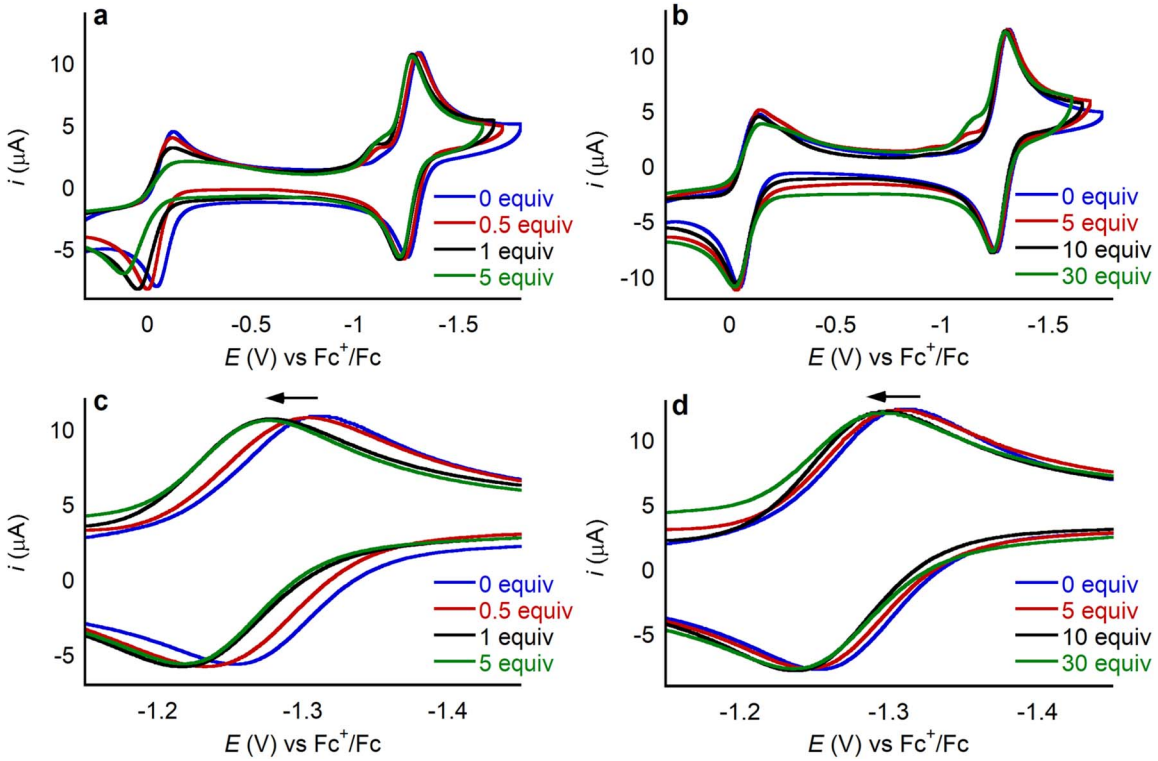


Fig. 7 Cyclic voltammograms collected at 100 mV $s^{-1}$ for 0.5 mM of **1** in 0.25 M $TBAPF_6$ in MeCN under an Ar atmosphere with increasing amounts of (a) $Ca(OTf)_2$ ($\Delta E_{1/2}$ = 34 mV at 1 equiv.) and (b) LiOTf ($\Delta E_{1/2}$ = 15 mV at 10 equiv.). (c) and (d) Zoom in of the $Co^{II}/Co^{I}$ couple in the presence of added $Ca(OTf)_2$ and LiOTf, respectively.

$Co^{I}$ redox couple stabilize after the addition of 1 equivalent of $Ca(OTf)_2$, whereas 10 equivalents are required for LiOTf. Likely, the $Co^{II}/Co^{I}$ reduction potential stops changing when all the available **1** is bound to the LA. Hence, the different number of equivalents of LA required for the reduction potential to stabilize is related to the different binding affinities of the LA to the aza-crown ether. Given that the aza-crown ether in **1** binds divalent cations more tightly than monocationic LAs (*vide supra*), it is not surprising that a lower number of equivalents of dicationic LAs is required for the change in reduction potential to stabilize. In the presence of LAs, there is a small peak preceding the $Co^{II}/Co^{I}$ reduction in **1** which may originate from some structural rearrangement or weak adsorption of the complex at the surface of the working electrode. Pre-waves in other transition metal based systems have been broadly interpreted in this way,[30] but we do not have experimental evidence to unambiguously assign this small peak. Rinse tests showed no residual features in the cyclic voltammogram, ruling out permanent adsorption of electroactive species to the working electrode.

The potential of the $Co^{III}/Co^{II}$ couple is also affected by the addition of the LA, as evidenced by the anodic shift observed in the presence of $Ca(OTf)_2$ (Fig. 6a). In the case of the $Co^{III}/Co^{II}$ couple, there is also change in the reversibility. For example, as the amount of $Ca(OTf)_2$ present increases there is an increase in the peak-to-peak separation for the reductive and oxidative voltammetric waves. In the absence of LA, we propose that the $Co^{III}/Co^{II}$ couple in **1** is only quasi-reversible because of the high reorganization energy associated with axial ligation changes (*vide supra*). We hypothesize that the solvent reorganization energy, which includes effects from solvent, electrolyte and LA salt, associated with the $Co^{III}/Co^{II}$ reduction of **1** is higher in the presence of LA. This slows electron transfer, which translates into a larger peak-to-peak separation as well as a decrease in peak current, particularly in the reductive wave.[31] The $Co^{III}/Co^{II}$ couple of **1** does not stop shifting at a given concentration of LA salt as seen for the $Co^{II}/Co^{I}$ couple and instead continues to shift anodically. Further, although the $Co^{II}/Co^{I}$ couple of the control compound **2** does not change upon the addition of LA, there is a small shift in the $Co^{III}/Co^{II}$ couple, especially for dicationic LAs (Fig. 6b). This shift is much smaller than what is observed for **1** but indicates there is likely some non-specific interaction of the LA with **2**. Altogether, for complex **1** the $Co^{III}/Co^{II}$ couple seems sensitive to bound and free LA, while the $Co^{II}/Co^{I}$ couple is only impacted by the LA ions bound to the aza-crown ether as shown in Fig. 7, hence we have centered our investigation on the $Co^{II}/Co^{I}$ couple of complexes **1** and **2**.

The observation that the $Co^{II}/Co^{I}$ couple remains reversible in the presence of LAs allows for the accurate determination of $E_{1/2}$ in the presence of LAs. We define $\Delta E_{1/2}$ as the maximum difference in the reduction potential of the $Co^{II}/Co^{I}$ couple of **1** in the presence and absence of LA. The maximum difference occurs when enough LA has been added so that the potential of the $Co^{II}/Co^{I}$ couple is no longer shifting and the change in reduction potential has reached its saturation point. We observe that dicationic LAs give bigger changes in $\Delta E_{1/2}$ than

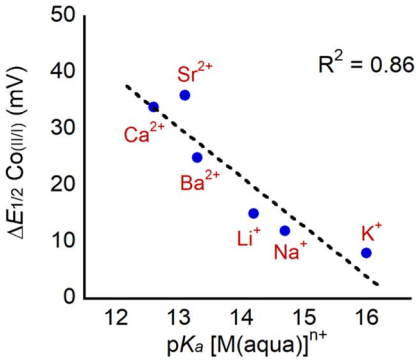


Fig. 8 Plot of $\Delta E_{1/2}$ for the $Co^{II}/Co^{I}$ couple in **1** upon LA binding as a function of the Lewis acidity of the cation, which is modelled using the p$K_a$ of the corresponding aqua complex.

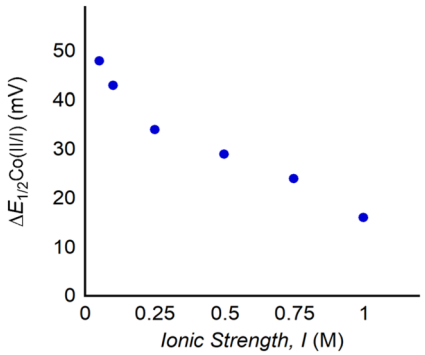


Fig. 9 Plot of $\Delta E_{1/2}$ for the $Co^{II}/Co^{I}$ couple of **1** with one equivalent of $Ca(OTf)_2$ at increasing $I$ ranging from 0.05 to 1.0 M $TBAPF_6$. Cyclic voltammograms are provided in Fig. S46.†

monocationic LAs, and the maximum shift that we observe is 38 mV in the case of $Sr^{2+}$. This change is significantly smaller than changes induced by LA binding in most other systems (for example, Yang and co-workers have observed shifts of up to 270 mV in modified Co Schiff base systems[5b]), likely because the LA is further away from the transition metal in **1** (*vide infra*). As observed previously, $\Delta E_{1/2}$ correlates with the Lewis acidity of the bound cations as shown in Fig. 8, when the Lewis acidity of the cation is modelled using the p$K_a$ of the aqua complex.[5b–d,5g,32] This suggests that electrostatic effects, namely the interaction between the Co center in **1** and the bound LA, are responsible for the differences in reduction potential upon LA binding. Unfortunately, **1** is not stable in the presence of tricationic LAs such as $Y^{3+}$ and $La^{3+}$(Fig. S44 and S45†), which would be expected to lead to even bigger changes in $\Delta E_{1/2}$.

It is interesting to compare our results to those obtained by Gilbertson and co-workers for an Fe complex containing a pyridinediimine ligand modified with a pendant 15-crown-5 ether (ligand **D** in Fig. 1) that binds $Na^+$ and $Li^+$ ions.[5a] In that study, the shift in the quasi-reversible $Fe^{II}/Fe^{I}$ couple upon $Na^+$ binding (in MeCN containing 0.1 M $TBAPF_6$) is approximately 14 mV, which is similar to the 12 mV shift we observe for **1** bound to $Na^+$. Importantly, the Fe–Na distance in the Fe complex is 6.85 Å in the solid state, while we estimate the Co–LA distance to range between 5.6 and 6.8 Å in our complexes based on DFT calculations (*vide infra*). When Gilbertson and co-workers shifted from MeCN, which has a high dielectric constant ($\varepsilon = 37.5$), to solvents with lower dielectric constants like dichloromethane ($\varepsilon = 8.93$) or tetrahydrofuran ($\varepsilon = 7.58$) the shift in reduction potential increased to approximately 50 mV for the $Na^+$ bound complex. This solvent dependence is consistent with our interpretation of long-range electrostatic effects being responsible for the changes in the reduction potential of the metal center, as the electric field caused by a point charge is inversely proportional to the dielectric constant of the medium in which the charged particle is immersed.

If electrostatic effects are responsible for the observed changes in reduction potential upon LA binding to **1**, it would be expected that the ionic strength ($I$) of the solution would influence $\Delta E_{1/2}$. This is because ions in solution can order around the **1**:LA adduct, and anions can dampen the electrostatic field created by the cationic LA. To modify the ionic strength ($I$) of the solution, we varied the concentration of the supporting electrolyte ($TBAPF_6$) and then recorded cyclic voltammograms of **1** with one equivalent of $Ca(OTf)_2$ (Fig. 9, S46 and Table S4†). The largest changes in $\Delta E_{1/2}$ for the $Co^{II}/Co^{I}$ couple are observed in solutions with the lowest ionic strength. In fact, a 35 mV difference in $\Delta E_{1/2}$ is observed between the lowest and highest ionic strength. Notably, this is almost as large as the changes observed in $\Delta E_{1/2}$ by varying the identity of the LA (*vide supra*). Apart from providing evidence for electrostatic effects being responsible for the shifts in reduction potential, this experiment is significant because to our knowledge it is the first example of the use of ionic strength to modulate the redox properties of a complex with an intramolecular LA binding site. Changing the ionic strength of the solution provides a new handle to tune the redox properties of the complex, which in some cases is easier than changing the LA and will give rise to a larger range of reduction potentials. Although lower ionic strengths lead to larger changes in reduction potential, in electrochemical processes it is not recommended to use ionic strengths below 0.1 M. However, Co porphyrin complexes,[8–10] such as **1**, may be used in conjunction with chemical reductants, in the absence of an electrolyte. In this case, the changes to the reduction potential of **1** that occur with LA binding at low electrolyte concentration will be relevant.

## Computational studies

DFT calculations were performed to gain information about the structure and electronic properties of **1** both with and without LAs bound. As part of these calculations, we explored the different conformations of the pendant aza-crown ether group that may be present in solution. To reduce the computational cost, the mesityl groups on the porphyrin were replaced by methyl groups. The resulting compound is denoted **1***. Initially, we sampled the possible conformations of one electron reduced **1*** (*i.e.*, $Co^{I}$ instead of $Co^{II}$) with $Ca^{2+}$ bound to the aza-crown ether group. We selected $Co^{I}$ instead of $Co^{II}$ both because it is diamagnetic, which leads to faster calculations, and because

solvent binding does not need to be considered for a square-planar 16-electron complex. Further, given that the cyclic voltammograms of **1** are reversible between $Co^{II}$ and $Co^{I}$, large conformational changes between complexes in the two oxidation states are likely not occurring. We used the Conformer-Rotamer Ensemble Sampling Tool (CREST)[33] to identify 159 conformers of reduced **1*** with $Ca^{2+}$ bound that are local minima at the density functional tight binding (DFTB) level of theory[34] in implicit acetonitrile solvent. The Co–$Ca^{2+}$ distance in these conformers span a wide range, from 5 to 14 Å. The LA-bound aza-crown ether moiety can fold so that is above the porphyrin plane, resulting in a Co–$Ca^{2+}$ distance close to 5 Å, or the arm connecting the aza-crown ether group to the porphyrin can fully extend, resulting in a much longer Co–$Ca^{2+}$ distance of ~14 Å (Fig. S47†). Among these conformers, we selected 12 geometrically distinct structures for further investigation at a higher computational level with the Co center in the paramagnetic $Co^{II}$ oxidation state. The selected structures were optimized at the DFT level of theory using the BP86 functional[35] in implicit acetonitrile solvent both with and without an explicit acetonitrile solvent molecule coordinated to Co. The free energy of each conformer was calculated, including zero-point energy and entropic contributions. Additional computational details are provided in the ESI.†

The relative stabilities of the selected conformers were characterized by their relative free energies, $\Delta G_{rel}$, where the free energy of the most stable conformer studied was used as the reference at 0 kcal mol$^{-1}$. The results for **1*** with various LAs bound to the aza-crown ether (**1***-LA) are shown in Fig. 10a. In these calculations, the axial acetonitrile ligand, expected to be bound in $Co^{II}$ porphyrins,[31] was not included to reduce the computational cost. Control calculations on both **1***-$Ca^{2+}$ and **1***-$Li^{+}$ indicated that the same trends were observed in the presence and absence of an axial ligand (Fig. S48†). Comparison of the different conformers of **1***-$Ca^{2+}$ indicates that there is an increase in the relative free energy as a function of the Co–$Ca^{2+}$ distance. The change in $\Delta G_{rel}$ with respect to the Co–$Ca^{2+}$ distance can be approximately described by a $1/d_{Co-LA}$ relation (dashed line in Fig. 10a), where $d_{Co-LA}$ is the distance between the Co and $Ca^{2+}$ centers. The structure of the most stable conformer for **1***-$Ca^{2+}$ is shown in Fig. 10b. Despite the repulsion between the positively charged $Co^{II}$ and the $Ca^{2+}$, the LA-bound aza-crown ether prefers to fold onto the porphyrin plane. Presumably, the repulsive interaction between the two cations is attenuated by the aza-crown ether group, and the attractive dispersion interactions between the porphyrin and the aza-crown ether groups are dominant. This leads to a net attraction between the $Ca^{2+}$-bound aza-crown ether and the Co porphyrin. Conformers similar to the lowest free energy structure of **1***-$Ca^{2+}$ (shown in Fig. 10b) are found to be the most stable for the other five LAs (Fig. S49†), and the same increase in free energy with increasing distance between the metal centers is observed. For all systems, the free energy difference between the most stable conformer and the others is well beyond the thermal energy at room temperature (0.6 kcal mol$^{-1}$). We therefore expect that only the most stable conformers exist in solution, with corresponding Co–LA distances ranging from 5.6 to 6.8 Å. The distance is shortest in **1**-$Li^{+}$ and largest in **1**-$Ba^{2+}$, as shown in Fig. 10a, which likely reflects the size of the cations.

We also calculated the relative reduction potential of the $Co^{II}/Co^{I}$ couple of **1*** for each LA using both the most stable geometry and the geometry with an extended arm (Fig. S47†). The $Co^{II}/Co^{I}$ reduction potential with no LA bound is used as the reference.[36] As shown in Fig. 11a, for the most stable conformer, we observe a roughly linear relationship between the relative reduction potential and the LA strength (expressed as the p$K_a$ of the corresponding aqua-complex). Apart from the reduction potential of **1***-$Ba^{2+}$, which is an outlier, the results agree qualitatively with our experimental observations. However, the calculated relative reduction potentials are one order of magnitude larger than the experimental results. We found that this disparity could be partially due to the absence of electrolyte in the computational model (see ESI†). Another source of error in the calculations is that the harmonic

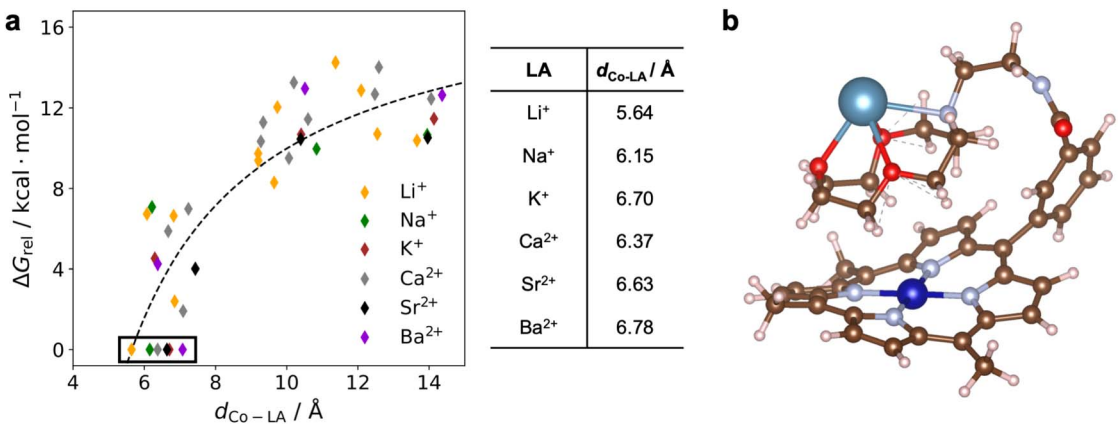


| LA | $d_{Co-LA}$ / Å |
|---|---|
| $Li^{+}$ | 5.64 |
| $Na^{+}$ | 6.15 |
| $K^{+}$ | 6.70 |
| $Ca^{2+}$ | 6.37 |
| $Sr^{2+}$ | 6.63 |
| $Ba^{2+}$ | 6.78 |

Fig. 10 (a) DFT calculated relative free energies of various conformers sampled for complex **1*** with different LAs as a function of the Co–LA distance. The axial acetonitrile ligand was not included in these calculations. The most stable conformers are indicated by the black box with their Co–LA distances listed in the table. The black dashed line is used to guide the eye. (b) Optimized geometry of the lowest free energy conformer of **1***-$Ca^{2+}$.

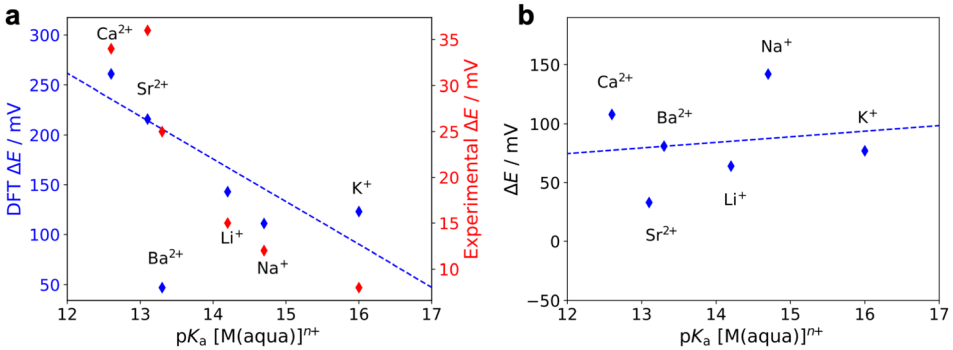


Fig. 11 Calculated relative reduction potentials (blue) of the $Co^{II}/Co^{I}$ couple of **1*** when LAs are bound to the aza-crown ether as a function of the LA strength. These calculations were performed for (a) the most stable geometry ('folded', as shown in Fig. 10b) and (b) the geometry with an extended arm, as in Fig. S42.† $\Delta E$ is the reduction potential for the **1***-LA species relative to the reduction potential of **1*** with no LA bound in either the folded or extended arm geometry. An axial acetonitrile ligand was explicitly included for the $Co^{II}$ species in these calculations. The data for $Ba^{2+}$ is excluded in both linear fits. A second *y* axis in (a) shows the experimental values (red) measured *via* cyclic voltammetry.

approximation was used to compute the zero-point energy and vibrational entropic contributions in the free energy calculations. Since both the porphyrin and the aza-crown ether groups are flexible, the vibrational modes of **1*** tend to have strong anharmonic character. Moreover, we replaced the mesityl groups by methyl groups in the calculations. The lower steric bulk of the methyl groups may result in a shorter Co–LA distance than for **1** and therefore may lead to larger reduction potential changes. In contrast to our results with the most stable 'folded' geometry, for the geometry with an extended arm, no trend is observed between the $Co^{II}/Co^{I}$ reduction potential and LA strength, as shown in Fig. 11b. The absence of any trend in the extended-arm geometry provides further support that the complexes adopt a folded geometry. Our conclusions also hold without an axial ligand bound to the $Co^{II}$ species (Fig. S49 and S50†).

Using the most stable geometry for each **1***-LA system, the electrostatic potential generated by the LA near the Co center, $\Delta\phi$, was calculated. This quantity $\Delta\phi$ is defined as the difference between the total electrostatic potentials of **1***-LA and **1*** at the DFT-optimized geometry of **1***-LA. Fig. 12a shows a typical electrostatic potential change caused by the bound $Ca^{2+}$ ion in the **1***-$Ca^{2+}$ adduct. A deeper shade of blue indicates a stronger, more positive, potential. The $\Delta\phi$ generated by different LAs can be quantitatively compared by taking the average within a 1 Å sphere near the Co ion (the ionic radius of $Co^{II}$ is about 0.7 Å)[37] as shown in Fig. 12b. Given that $\Delta\phi$ is determined by subtracting the total electrostatic potentials of two structures that differ only by the presence of the cationic LA, $\Delta\phi$ reflects the electrostatic effect of a point charge. This explains why the $\Delta\phi$ values for the divalent cations are approximately double those for the monovalent cations. The differences between LA cations of equal charge arise from the different Co–LA distances determined from geometry optimizations of **1***-LA and the different ionic radii of the LA cations. Altogether, this relatively simple calculation yields $\Delta\phi$ values that correlate well with the LA strength (Fig. 12b), showing a trend similar to that obtained in our electrochemical experiments (Fig. 8). Our calculations offer proposed geometries for the **1**-LA complexes and provide strong support for the hypothesis that the observed changes in

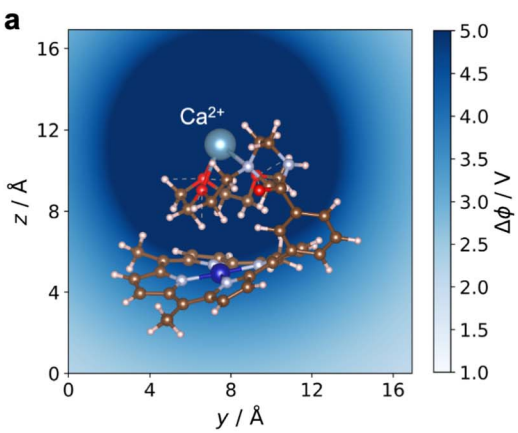


| LA | ΔΦ / V |
|---|---|
| $Li^+$ | 2.56 |
| $Na^+$ | 2.37 |
| $K^+$ | 2.20 |
| $Ca^{2+}$ | 4.57 |
| $Sr^{2+}$ | 4.41 |
| $Ba^{2+}$ | 4.27 |

Fig. 12 (a) Electrostatic potential ($\Delta\phi$) generated by $Ca^{2+}$ in **1***-$Ca^{2+}$. (b) Calculated $\Delta\phi$ generated by the LA at the Co center in **1***-LA as a function of the LA strength.

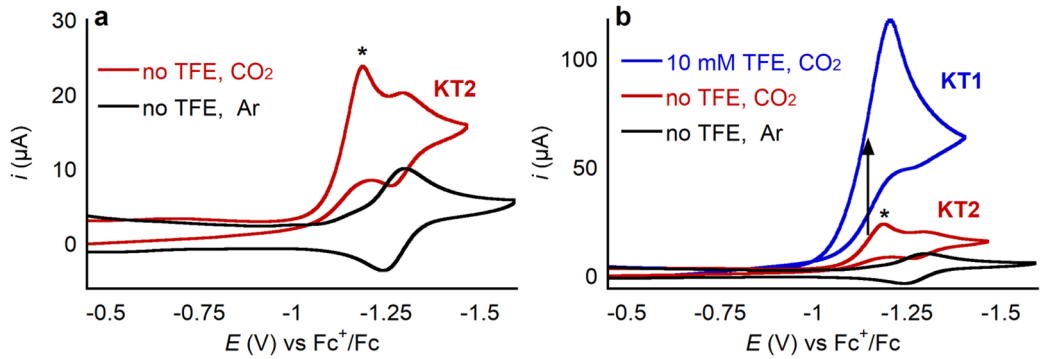


Fig. 13 CV of 0.5 mM **1** at 100 mV $s^{-1}$ in 0.25 M $TBAPF_6$/MeCN under 1 atm of the specified gas, (a) without added proton source (TFE, p$K_a$ = 35.4) and (b) with 10 mM of trifluoroethanol.

the redox properties of **1** upon LA binding are related to electrostatic effects.

### Electrocatalytic $CO_2$ reduction by 1

$Co^{II}$ porphyrin complexes are well-known electrocatalysts for $CO_2$ reduction, often giving selective conversion to CO.[38] Therefore, we explored the ability of **1** to electrocatalytically reduce $CO_2$ with the goal of ultimately assessing whether binding of a cationic LA impacts catalysis. A cyclic voltammogram of **1** under $CO_2$ shows the same $Co^{III}/Co^{II}$ and $Co^{II}/Co^{I}$ waves described earlier. In addition, there is an irreversible peak approximately 100 mV anodic of the $Co^{II}/Co^{I}$ couple as shown in Fig. 13a, where the new catalytic peak is labeled with an asterisk. This behavior is consistent with a total catalysis regime, specifically the cyclic voltammogram shows the characteristic shape of a KT2 voltammogram as described in Savéant's Kinetic Zone diagram.[39] A cyclic voltammogram exhibits a KT2 shape because the rate of catalysis is so fast that even a small fraction of the catalyst in the reduced active form is able to consume all of the substrate, or co-substrate, available in the reaction-diffusion layer quickly. Then, when the potential of the catalysis-initiating redox couple is reached there is no substrate for the catalyst to use and thus the reversible wave is observed. Addition of 10 mM of the Brønsted acid trifluoroethanol (TFE) led to a significant current increase of the catalytic peak, effectively moving the cyclic voltammogram into a KT1 regime (Fig. 13b).[39] In this case, the higher concentration of co-substrate (*i.e.*, proton donor, TFE) allows for catalysis to be sustained for longer, so a larger catalytic peak grows that completely obscures the reversible $Co^{II}/Co^{I}$ couple.

Despite the cyclic voltammogram of **1** indicating fast initial electrocatalytic $CO_2$ reduction, the complex is unstable under electrocatalytic conditions. When further cyclic voltammograms are collected, the catalytic current diminishes rapidly (Fig. S51†), consistent with loss of catalytic activity, which precluded running controlled potential electrolysis (CPE) experiments to determine the product distribution. Similarly, when the electrocatalytic performance of **1** was evaluated in the presence of LAs, such as $Ca(OTf)_2$, even though there was an initial large increase in current under $CO_2$, rapid catalyst decomposition was observed, preventing detailed analysis. We hypothesize that the nitrogen atom in the aza-crown ether reacts with $CO_2$ leading to a loss of $CO_2$-reduction activity. Consistent with this proposal, the control compound **2** generates significant quantities of CO in electrocatalytic experiments, is stable for over 2 hours of CPE, and displays a stable current (Fig. S52 and S53†). Further, chemical reduction of **1** by $KC_8$ followed by exposure to $CO_2$ leads to formation of a precipitate and a discoloration of the solution. On the other hand, when **2** is treated similarly, it remains in solution with no color change and yields a $^1H$ NMR spectrum consistent with a one-electron reduced $CO_2$-bound species that remains stable for at least 18 hours. Future efforts will be directed toward the synthesis of metalloporphyrin–crown ether complexes that are stable under $CO_2$ to explore the impact of bound LAs in electrocatalytic $CO_2$ reduction.

## Conclusions

We have prepared a $Co^{II}$ porphyrin complex, **1**, which contains a pendant aza-crown ether group that can bind cationic Group I and II LAs to change the internal electric field. The binding constant for $Li^+$ coordination is similar to free aza-crown ethers, whereas other metal complexes containing pendant aza-crown or crown ether ligands often have significantly lower binding affinities for LAs.[5e,27] This is likely because the aza-crown ether group in **1** is remote from the Co center, and none of the atoms associated with the aza-crown ether interact directly with the Co. Strong LA binding is potentially important in electrocatalytic $CO_2$ reduction, where the use of a lower number of equivalents of LA is expected to result in less electrode fouling due to the formation of insoluble carbonates.

LA binding causes an anodic shift in both the $Co^{III}/Co^{II}$ and $Co^{II}/Co^{I}$ redox couples of **1**. The magnitude of the $Co^{II}/Co^{I}$ shift varies predictably with the LA strength of the bound cation, increasing linearly with the p$K_a$ of the corresponding metal–aqua complex. This result is consistent with previous literature reports,[4f,j,5d,g,32b] but the magnitude of the shift is smaller than the shifts found for systems in which the LA is positioned closer (~3 Å) to the metal center.[4f,5d,5f,g] Our DFT studies imply that the distance between the bound LA and the Co center ranges from 5.6 to 6.8 Å, suggesting that the effects seen in the

electrochemical properties of **1** are due to long-range electrostatic interactions. The calculated electrostatic potential generated by the LA near the Co center is also linearly correlated with the p$K_a$ of the corresponding metal–aqua complex. Moreover, the magnitude of the shift in the $Co^{II}/Co^{I}$ couple upon LA binding is sensitive to the ionic strength of the solution, with solutions containing higher electrolyte concentration resulting in smaller changes in reduction potential. To our knowledge this is the first time that the ionic strength of the solution has been used as a handle to tune the redox properties of transition metal complexes with intramolecular electric fields. Although the CV response of **1** suggests fast $CO_2$ reduction catalysis, the complex quickly deactivates under $CO_2$, which we attribute to the nitrogen atom in the aza-crown ether group reacting with $CO_2$.

Overall, we have developed a Co porphyrin system in which the redox properties can be tuned *via* long-range electrostatic effects. Importantly, it is likely that using this system it will be possible to independently modulate the primary coordination sphere and the internal electric field. Future research efforts will be dedicated to the synthesis of structurally related complexes with crown ether groups that are expected to be more stable under the conditions used for electrocatalytic $CO_2$ reduction and will allow catalytic performance to be evaluated as both the primary coordination sphere and magnitude of the internal electric field are varied.

## Data availability

The datasets supporting this article have been uploaded as part of the ESI.†

## Author contributions

JLAH: conceptualization, investigation, experimental methodology, writing – original draft. XZ: investigation, synthetic methodology, writing – original draft (synthesis). KC: conceptualization, investigation, computational methodology, writing – original draft (computational studies). APD: investigation. SHS: conceptualization, supervision, writing – review and editing. NH: conceptualization, supervision, writing – review and editing. NP: investigation. MZ: conceptualization, supervision, writing – review and editing.

## Conflicts of interest

There are no conflicts to declare.

## Acknowledgements

This work was solely supported as part of the Center for Hybrid Approaches in Solar Energy to Liquid Fuels (CHASE), an Energy Innovation Hub funded by the U.S. Department of Energy, Office of Science, Office of Basic Energy Sciences under Award Number DE-SC0021173. NH & MZ thank the Yale Planetary Solutions Project for assistance. We thank Prof. Gary Brudvig and Prof. Hailiang Wang for helpful discussions, and Dr Reagan Hooper for assistance with EPR simulations.

## References

1 (*a*) J. A. Gerlt, M. M. Kreevoy, W. W. Cleland and P. A. Frey, Understanding Enzymic Catalysis: The Importance of Short, Strong Hydrogen Bonds, *Chem. Biol.*, 1997, **4**, 259; (*b*) G. J. Bartlett, C. T. Porter, N. Borkakoti and J. M. Thornton, Analysis of Catalytic Residues in Enzyme Active Sites, *J. Mol. Biol.*, 2002, **324**, 105; (*c*) S. D. Fried, S. Bagchi and S. G. Boxer, Extreme Electric Fields Power Catalysis in the Active Site of Ketosteroid Isomerase, *Science*, 2014, **346**, 1510; (*d*) S. D. Fried and S. G. Boxer, Measuring Electric Fields and Noncovalent Interactions Using the Vibrational Stark Effect, *Acc. Chem. Res.*, 2015, **48**, 998; (*e*) P. Hanoian, C. T. Liu, S. Hammes-Schiffer and S. Benkovic, Perspectives on Electrostatics and Conformational Motions in Enzyme Catalysis, *Acc. Chem. Res.*, 2015, **48**, 482; (*f*) Y. Wu and S. G. Boxer, A Critical Test of the Electrostatic Contribution to Catalysis with Noncanonical Amino Acids in Ketosteroid Isomerase, *J. Am. Chem. Soc.*, 2016, **138**, 11890; (*g*) S. D. Fried and S. G. Boxer, Electric Fields and Enzyme Catalysis, *Annu. Rev. Biochem.*, 2017, **86**, 387; (*h*) Y.-W. Lin, Rational Design of Metalloenzymes: From Single to Multiple Active Sites, *Coord. Chem. Rev.*, 2017, **336**, 1.

2 (*a*) J. Bonin, C. Costentin, C. Robert, J.-M. Savéant and C. Tard, Hydrogen-Bond Relays in Concerted Proton-Electron Transfers, *Acc. Chem. Res.*, 2011, **45**, 372; (*b*) S. A. Cook and A. S. Borovik, Molecular Designs for Controlling the Local Environments around Metal Ions, *Acc. Chem. Res.*, 2015, **48**, 2407; (*c*) K. T. Mahmudov, M. N. Kopylovich, M. F. C. Guedes da Silva and A. J. L. Pombeiro, Non-Covalent Interactions in the Synthesis of Coordination Compounds: Recent Advances, *Coord. Chem. Rev.*, 2017, **345**, 54; (*d*) L. V. Hale and N. K. Szymczak, Hydrogen Transfer Catalysis Beyond the Primary Coordination Sphere, *ACS Catal.*, 2018, **8**, 6446.

3 (*a*) A. D. Wilson, R. H. Newell, M. J. McNevin, J. T. Muckerman, M. R. DuBois and D. L. DuBois, Hydrogen Oxidation and Production Using Nickel-Based Molecular Catalysts with Positioned Proton Relays, *J. Am. Chem. Soc.*, 2006, **128**, 358; (*b*) J. Y. Yang, S. E. Smith, T. Liu, W. G. Dougherty, W. A. Hoffert, W. S. Kassel, M. R. DuBois, D. L. DuBois and R. M. Bullock, Two Pathways for Electrocatalytic Oxidation of Hydrogen by a Nickel Bis(diphosphine) Complex with Pendant Amines in the Second Coordination Sphere, *J. Am. Chem. Soc.*, 2013, **135**, 9700; (*c*) C. Costentin, G. Passard, M. Robert and J.-M. Savéant, Pendant Acid–Base Groups in Molecular Catalysts: H-Bond Promoters or Proton Relays? Mechanisms of the Conversion of $CO_2$ to CO by Electrogenerated Iron(0)Porphyrins Bearing Prepositioned Phenol Functionalities, *J. Am. Chem. Soc.*, 2014, **136**, 11821; (*d*) S. E. Creutz and J. C. Peters, Exploring Secondary-Sphere Interactions in Fe–$N_xH_y$ Complexes Relevant to $N_2$

Fixation, *Chem. Sci.*, 2017, **8**, 2321; (*e*) S. Roy, B. Sharma, J. Pécaut, P. Simon, M. Fontecave, P. D. Tran, E. Derat and V. Artero, Molecular Cobalt Complexes with Pendant Amines for Selective Electrocatalytic Reduction of Carbon Dioxide to Formic Acid, *J. Am. Chem. Soc.*, 2017, **139**, 3685; (*f*) H. Sun, Y. Han, H. Lei, M. Chen and R. Cao, Cobalt Corroles with Phosphonic acid Pendants as Catalysts for Oxygen and Hydrogen Evolution From Neutral Aqueous Solution, *Chem. Commun.*, 2017, **53**, 6195; (*g*) T. Z. H. Gani and H. J. Kulik, Understanding and Breaking Scaling Relations in Single-Site Catalysis: Methane to Methanol Conversion by FeIV=O, *ACS Catal.*, 2018, **8**, 975; (*h*) E. M. Nichols, J. S. Derrick, S. K. Nistanaki, P. T. Smith and C. J. Chang, Positional Effects of Second-Sphere Amide Pendants on Electrochemical $CO_2$ Reduction Catalyzed by Iron Porphyrins, *Chem. Sci.*, 2018, **9**, 2952; (*i*) D. Dolui, S. Khandelwal, A. Shaik, D. Gaat, V. Thiruvenkatam and A. Dutta, Enzyme-Inspired Synthetic Proton Relays Generate Fast and Acid-Stable Cobalt-Based $H_2$ Production Electrocatalysts, *ACS Catal.*, 2019, **9**, 10115; (*j*) A. Chapovetsky, M. Welborn, J. M. Luna, R. Haiges, T. F. Miller III and S. C. Marinescu, Pendant Hydrogen-Bond Donors in Cobalt Catalysts Independently Enhance $CO_2$ Reduction, *ACS Cent. Sci.*, 2018, **4**, 397; (*k*) N. Queyriaux, D. Sun, J. Fize, J. Pécaut, M. J. Field, M. Chavarot-Kerlidou and V. Artero, Electrocatalytic Hydrogen Evolution with a Cobalt Complex Bearing Pendant Proton Relays: Acid Strength and Applied Potential Govern Mechanism and Stability, *J. Am. Chem. Soc.*, 2020, **142**, 274; (*l*) S. Bhunia, A. Rana, S. Hematian, K. D. Karlin and A. Dey, Proton Relay in Iron Porphyrins for Hydrogen Evolution Reaction, *Inorg. Chem.*, 2021, **60**, 13876; (*m*) S. Bhunia, A. Ghatak, A. Rana and A. Dey, Amine Groups in the Second Sphere of Iron Porphyrins Allow for Higher and Selective $4e^-/4H^+$ Oxygen Reduction Rates at Lower Overpotentials, *J. Am. Chem. Soc.*, 2023, **145**, 3812; (*n*) J. S. Derrick, M. Loipersberger, S. K. Nistanaki, A. V. Rothweiler, M. Head-Gordon, E. M. Nichols and C. J. Chang, Templating Bicarbonate in the Second Coordination Sphere Enhances Electrochemical $CO_2$ Reduction Catalyzed by Iron Porphyrins, *J. Am. Chem. Soc.*, 2022, **144**, 11656.

4 (*a*) C. F. Gorin, E. S. Beh and M. W. Kanan, An Electric Field–Induced Change in the Selectivity of a Metal Oxide–Catalyzed Epoxide Rearrangement, *J. Am. Chem. Soc.*, 2012, **134**, 186; (*b*) C. F. Gorin, E. S. Beh, Q. M. Bui, G. R. Dick and M. W. Kanan, Interfacial Electric Field Effects on a Carbene Reaction Catalyzed by Rh Porphyrins, *J. Am. Chem. Soc.*, 2013, **135**, 11257; (*c*) I. Azcarate, C. Costentin, M. Robert and J.-M. Savéant, Through-Space Charge Interaction Substituent Effects in Molecular Catalysis Leading to the Design of the Most Efficient Catalyst of $CO_2$-to-CO Electrochemical Conversion, *J. Am. Chem. Soc.*, 2016, **138**, 16639; (*d*) S. Shaik, D. Mandal and R. Ramanan, Oriented Electric Fields as Future Smart Reagents in Chemistry, *Nat. Chem.*, 2016, **8**, 1091; (*e*) V. M. Lau, W. C. Pfalzgraff, T. E. Markland and M. W. Kanan, Electrostatic Control of Regioselectivity in Au(I)-Catalyzed Hydroarylation, *J. Am. Chem. Soc.*, 2017, **139**, 4035; (*f*) T. Chantarojsiri, J. W. Ziller and J. Y. Yang, Incorporation of Redox-Inactive Cations Promotes Iron Catalyzed Aerobic C–H Oxidation at Mild Potentials, *Chem. Sci.*, 2018, **9**, 2567; (*g*) S. Ciampi, N. Darwish, H. M. Aitken, I. Díez-Pérez and M. L. Coote, Harnessing Electrostatic Catalysis in Single Molecule, Electrochemical and Chemical Systems: A Rapidly Growing Experimental Tool Box, *Chem. Soc. Rev.*, 2018, **47**, 5146; (*h*) C. G. Margarit, N. G. Asimow, M. I. Gonzalez and D. G. Nocera, Double Hangman Iron Porphyrin and the Effect of Electrostatic Nonbonding Interactions on Carbon Dioxide Reduction, *J. Phys. Chem. Lett.*, 2020, **11**, 1890; (*i*) D. J. Martin and J. M. Mayer, Oriented Electrostatic Effects on $O_2$ and $CO_2$ Reduction by a Polycationic Iron Porphyrin, *J. Am. Chem. Soc.*, 2021, **143**, 11423; (*j*) N. G. Léonard, R. Dhaoui, T. Chantarojsiri and J. Y. Yang, Electric Fields in Catalysis: From Enzymes to Molecular Catalysts, *ACS Catal.*, 2021, **11**, 10923; (*k*) A. B. Weberg, S. P. McCollom, L. M. Thierer, M. R. Gau, P. J. Carroll and N. C. Tomson, Using Internal Electrostatic Fields to Manipulate the Valence Manifolds of Copper Complexes, *Chem. Sci.*, 2021, **12**, 4395; (*l*) A. B. Weberg, R. P. Murphy and N. C. Tomson, Oriented Internal Electrostatic Fields: an Emerging Design Element in Coordination Chemistry and Catalysis, *Chem. Sci.*, 2022, **13**, 5432.

5 (*a*) M. Delgado, J. M. Ziegler, T. Seda, L. N. Zakharov and J. D. Gilbertson, Pyridinediimine Iron Complexes with Pendant Redox-Inactive Metals Located in the Secondary Coordination Sphere, *Inorg. Chem.*, 2016, **55**, 555; (*b*) A. H. Reath, J. W. Ziller, C. Tsay, A. J. Ryan and J. Y. Yang, Redox Potential and Electronic Structure Effects of Proximal Nonredox Active Cations in Cobalt Schiff Base Complexes, *Inorg. Chem.*, 2017, **56**, 3713; (*c*) K. Kang, J. Fuller, A. H. Reath, J. W. Ziller, A. N. Alexandrova and J. Y. Yang, Installation of Internal Electric Fields by Non-Redox Active Cations in Transition Metal Complexes, *Chem. Sci.*, 2019, **10**, 10135; (*d*) A. Kumar, D. Lionetti, V. W. Day and J. D. Blakemore, Redox-Inactive Metal Cations Modulate the Reduction Potential of the Uranyl Ion in Macrocyclic Complexes, *J. Am. Chem. Soc.*, 2020, **142**, 3032; (*e*) N. S. Idris, J. M. Barlow, S. A. Chabolla, J. W. Ziller and J. Y. Yang, Synthesis and Redox Properties of Heterobimetallic $Re(bpy^{Crown\text{-}M})(CO)_3Cl$ Complexes, where M = $Na^+$, $K^+$, $Ca^{2+}$, and $Ba^{2+}$, *Polyhedron*, 2021, **208**, 115385; (*f*) N. G. Léonard, T. Chantarojsiri, J. W. Ziller and J. Y. Yang, Cationic Effects on the Net Hydrogen Atom Bond Dissociation Free Energy of High-Valent Manganese Imido Complexes, *J. Am. Chem. Soc.*, 2022, **144**, 1503; (*g*) R. R. Golwankar, A. Kumar, V. W. Day and J. D. Blakemore, Revealing the Influence of Diverse Secondary Metal Cations on Redox-Active Palladium Complexes, *Chem.–Eur. J.*, 2022, **28**, e202200344; (*h*) H. M. Nguyen, H. W. T. Morgan, T. Chantarojsiri, T. A. Kerr, J. Y. Yang, A. N. Alexandrova and N. G. Léonard, Charge and Solvent Effects on the Redox Behavior of Vanadyl Salen–Crown Complexes, *J. Phys. Chem. A*, 2023, **127**, 5324.

6 (*a*) J. W. Steed, First-and Second-Sphere Coordination Chemistry of Alkali Metal Crown Ether Complexes, *Coord. Chem. Rev.*, 2001, **215**, 171; (*b*) G. W. Gokel, W. M. Leevy and M. E. Weber, Crown Ethers: Sensors for Ions and Molecular Scaffolds for Materials and Biological Models, *Chem. Rev.*, 2004, **104**, 2723; (*c*) X. Chen, F. Wang, J. Y. Hyun, T. Wei, J. Qiang, X. Ren, I. Shin and J. Yoon, Recent Progress in the Development of Fluorescent, Luminescent and Colorimetric Probes or Detection of Reactive Oxygen and Nitrogen Species, *Chem. Soc. Rev.*, 2016, **45**, 2976.

7 S. Acosta-Calle and A. J. M. Miller, Tunable and Switchable Catalysis Enabled by Cation-Controlled Gating with Crown Ether Ligands, *Acc. Chem. Res.*, 2023, **56**, 971.

8 (*a*) G. F. Manbeck and E. Fujita, A Review of Iron and Cobalt Porphyrins, Phthalocyanines and Related Complexes for Electrochemical and Photochemical Reduction of Carbon Dioxide, *J. Porphyrins Phthalocyanines*, 2015, **19**, 45; (*b*) P. Gotico, Z. Halime and A. Aukauloo, Recent Advances in Metalloporphyrin-Based Catalyst Design Towards Carbon Dioxide Reduction: From Bio-Inspired Second Coordination Sphere Modifications to Hierarchical Architectures, *Dalton Trans.*, 2020, **49**, 2381; (*c*) Z. Liang, H.-Y. Wang, H. Zheng, W. Zhang and R. Cao, Porphyrin-Based Frameworks for Oxygen Electrocatalysis and Catalytic Reduction of Carbon Dioxide, *Chem. Soc. Rev.*, 2021, **50**, 2540.

9 (*a*) W. Zhang, W. Lai and R. Cao, Energy-Related Small Molecule Activation Reactions: Oxygen Reduction and Hydrogen and Oxygen Evolution Reactions Catalyzed by Porphyrin-and Corrole-Based Systems, *Chem. Rev.*, 2017, **117**, 3717; (*b*) S. Bhunia, A. Ghatak and A. Dey, Second Sphere Effects on Oxygen Reduction and Peroxide Activation by Mononuclear Iron Porphyrins and Related Systems, *Chem. Rev.*, 2022, **122**, 12370.

10 B. B. Beyene and C.-H. Hung, Recent Progress on Metalloporphyrin-Based Hydrogen Evolution Catalysis, *Coord. Chem. Rev.*, 2020, **410**, 213234.

11 Y. Zhao, M. Yu and X. Fu, Photo-Cleavage of the Cobalt–Carbon Bond: Visible Light-Induced Living Radical Polymerization Mediated by Organo-Cobalt Porphyrins, *Chem. Commun.*, 2013, **49**, 5186.

12 (*a*) H. Lu and X. P. Zhang, Catalytic C–H Functionalization by Metalloporphyrins: Recent Developments and Future Directions, *Chem. Soc. Rev.*, 2011, **40**, 1899; (*b*) C.-M. Che, V. K.-Y. Lo, C.-Y. Zhou and J.-S. Huang, Selective Functionalisation of Saturated C–H Bonds with Metalloporphyrin Catalysts, *Chem. Soc. Rev.*, 2011, **40**, 1950.

13 (*a*) E. Rose, B. Andrioletti, S. Zrig and M. Quelquejeu-Ethève, Enantioselective Epoxidation of Olefins with Chiral Metalloporphyrin Catalysts, *Chem. Soc. Rev.*, 2005, **34**, 573; (*b*) Q.-H. Xia, H.-Q. Ge, C.-P. Ye, Z.-M. Liu and K.-X. Su, Advances in Homogeneous and Heterogeneous Catalytic Asymmetric Epoxidation, *Chem. Rev.*, 2005, **105**, 1603.

14 (*a*) B. Meunier, Metalloporphyrins as Versatile Catalysts for Oxidation Reactions and Oxidative DNA Cleavage, *Chem. Rev.*, 1992, **92**, 1411; (*b*) M. Pagliaro, S. Campestrini and R. Ciriminna, Ru-Based Oxidation Catalysis, *Chem. Soc. Rev.*, 2005, **34**, 837.

15 (*a*) V. Thanabal and V. Krishnan, Porphyrins with Multiple Crown Ether Voids: Novel Systems for Cation Complexation Studies, *J. Am. Chem. Soc.*, 1982, **104**, 3643; (*b*) H. Van Willigen and T. Chandrashekar, ENDOR Study of Copper(II) Crown Porphyrin Dimerization, *J. Am. Chem. Soc.*, 1986, **108**, 709; (*c*) H. Shinmori and A. Osuka, Extended Molecular Assembly of Crown Ether Appended Meso–Meso Coupled Diporphyrin, *Tetrahedron Lett.*, 2000, **41**, 8527; (*d*) H. Shinmori, H. Furuta and A. Osuka, Effective Face-to-Face Dimerization of a Crown Ether Appended N-Confused Porphyrin, *Tetrahedron Lett.*, 2002, **43**, 4881; (*e*) M. Jahan, N. Safari, H. Khosravi, A. Moghimi and B. Notash, Crown Ether-Appended Porphyrins and Metalloporphyrins: Synthesis, Characterization and Metal Ions Interaction, *Polyhedron*, 2005, **24**, 1682; (*f*) P. Even and B. Boitrel, Crown Porphyrins, *Coord. Chem. Rev.*, 2006, **250**, 519; (*g*) E. A. Mikhalitsyna, V. S. Tyurin, I. A. Zamylatskov, V. N. Khrustalev and I. P. Beletskaya, Synthesis, Characterization and Cation-Induced Dimerization of New Aza-Crown Ether-Appended Metalloporphyrins, *Dalton Trans.*, 2012, **41**, 7624.

16 X. Zhang, F. Lin, M. Cao and M. Zhong, Rare Earth–Cobalt Bimetallic Catalysis Mediates Stereocontrolled Living Radical Polymerization of Acrylamides, *Nat. Synth.*, 2023, **2**, 855.

17 (*a*) P. Kuś, Tetraphenylporphyrins Monosubstituted with a Crown Ether in One Phenyl Ring. Synthesis and Characterization, *Monatsh. Chem.*, 1997, **128**, 911; (*b*) H. Tsukube, M. Wada, S. Shinoda and H. Tamiaki, Porphyrinatoerbium–Crown Ether Conjugate for Synergistic Binding and Chirality Sensing of Zwitterionic Amino Acids, *Chem. Commun.*, 1999, 1007; (*c*) S. Iwata, M. Suzuki, M. Shirakawa and K. Tanaka, Cation and Anion Recognition of Crown Ether-armed Metalloporphyrin, *Supramol. Chem.*, 1999, **11**, 135; (*d*) S. J. Lange, J. W. Sibert, A. G. M. Barrett and B. M. Hoffman, Synthesis and Coordination Chemistry of Unsymmetrical Tetraazaporphyrins Containing Single Oxathia- and Thiacrown Substituents, *Tetrahedron*, 2000, **56**, 7371; (*e*) Y. Chen and K. Wang, Azacrown[N,S,O]-Modified Porphyrin Sensor for Detection of $Ag^{+}$, $Pb^{2+}$, and $Cu^{2+}$, *Photochem. Photobiol. Sci.*, 2013, **12**, 2001.

18 (*a*) E. B. Fleischer, J. M. Palmer, T. S. Srivastava and A. Chatterjee, Thermodyamic and Kinetic Properties of an Iron-Porphyrin System, *J. Am. Chem. Soc.*, 1971, **93**, 3162; (*b*) T. Nakazono, A. R. Parent and K. Sakai, Cobalt Porphyrins as Homogeneous Catalysts for Water Oxidation, *Chem. Commun.*, 2013, **49**, 6325.

19 F. A. Tezcan, J. R. Winkler and H. B. Gray, Probing Protein Folding with Substitution-Inert Metal Ions. Folding Kinetics of Cobalt (III)-Cytochrome c, *J. Am. Chem. Soc.*, 1999, **121**, 11918.

20 R. Giovannetti, in *Macro to Nano Spectroscopy*, ed. J. Uddin, IntechOpen, 2012.

21 J. G. Kleingardner, B. Kandemir and K. L. Bren, Hydrogen Evolution From Neutral Water Under Aerobic Conditions Catalyzed by Cobalt Microperoxidase-11, *J. Am. Chem. Soc.*, 2014, **136**, 4.

22 G. Däges and J. Hüttermann, ESR and ENDOR of Pentacoordinated Cobalt(II) Porphyrins, *J. Phys. Chem.*, 1992, **96**, 4787.

23 (*a*) M. Isaacs, J. C. Canales, A. Riquelme, M. Lucero, M. J. Aguirre and J. Costamagna, Contribution of the Ligand to the Electroreduction of $CO_2$ Catalyzed by a Cobalt(II) Macrocyclic Complex, *J. Coord. Chem.*, 2003, **56**, 1193; (*b*) V. Artero, M. Chavarot-Kerlidou and M. Fontecave, Splitting Water with Cobalt, *Angew. Chem., Int. Ed.*, 2011, **50**, 7238; (*c*) B. H. Solis, A. G. Maher, T. Honda, D. C. Powers, D. G. Nocera and S. Hammes-Schiffer, Theoretical Analysis of Cobalt Hangman Porphyrins: Ligand Dearomatization and Mechanistic Implications for Hydrogen Evolution, *ACS Catal.*, 2014, **4**, 4516.

24 (*a*) E. Karkhaneei, A. Afkhami and M. Shamsipur, Nuclear Magnetic Resonance Study of Lithium Ion Complexes with Several Crown Ethers in Binary Acetonitrile-Nitromethane Mixtures, *J. Coord. Chem.*, 1996, **39**, 33; (*b*) M. Shamsipur and T. Madrakian, Competitive NMR Study of the Complexation of Some Alkaline Earth and Transition Metal Ions with 12-crown-4, 15-crown-5 and benzo-15-crown-5 in Acetonitrile Solution Using the Lithium-7 Nucleus as a Probe, *J. Coord. Chem.*, 1999, **52**, 139.

25 (*a*) P. Thordarson, Determining Association Constants from Titration Experiments in Supramolecular Chemistry, *Chem. Soc. Rev.*, 2010, **40**, 1305; (*b*) A. Kumar and J. D. Blakemore, On the Use of Aqueous Metal-Aqua p$K_a$ Values as a Descriptor of Lewis Acidity, *Inorg. Chem.*, 2021, **60**, 1107; (*c*) R. R. Golwankar, T. Davis Curry II, C. J. Paranjothi and J. D. Blakemore, Molecular Influences on the Quantification of Lewis Acidity with Phosphine Oxide Probes, *Inorg. Chem.*, 2023, **62**, 9765.

26 A. J. Smetana and A. I. Popov, Lithium-7 Nuclear Magnetic Resonance and Calorimetric Study of Lithium Crown Complexes in Various Solvents, *J. Solution Chem.*, 1980, **9**, 183.

27 J. B. Smith, A. M. Camp, A. H. Farquhar, S. H. Kerr, C.-H. Chen and A. J. M. Miller, Organometallic Elaboration as a Strategy for Tuning the Supramolecular Characteristics of Aza-Crown Ethers, *Organometallics*, 2019, **38**, 4392.

28 (*a*) M. Hammouche, D. Lexa, M. Momenteau and J.-M. Savéant, Chemical Catalysis of Electrochemical Reactions. Homogeneous Catalysis of the Electrochemical Reduction of Carbon Dioxide by lron("0") Porphyrins. Role of the Addition of Magnesium Cations, *J. Am. Chem. Soc.*, 1991, **113**, 8455; (*b*) M. D. Sampson and C. P. Kubiak, Manganese Electrocatalysts with Bulky Bipyridine Ligands: Utilizing Lewis Acids To Promote Carbon Dioxide Reduction at Low Overpotentials, *J. Am. Chem. Soc.*, 2016, **138**, 1386.

29 A. Zhanaidarova, H. Steger, M. H. Reineke and C. P. Kubiak, Chelated $[Zn(cyclam)]^{2+}$ Lewis Acid Improves the Reactivity of the Electrochemical Reduction of $CO_2$ by Mn Catalysts with Bulky Bipyridine Ligands, *Dalton Trans.*, 2017, **46**, 12413.

30 K. J. Lee, B. D. McCarthy and J. L. Dempsey, On Decomposition, Degradation, and Voltammetric Deviation: The Electrochemist's Field Guide to Identifying Precatalyst Transformation, *Chem. Soc. Rev.*, 2019, **48**, 2927.

31 J.-M. Savéant, Elements of Molecular and Biomolecular Electrochemistry, *An Electrochemical Approach to Electron Transfer Chemistry*, John Wiley & Sons, 2006.

32 (*a*) E. Y. Tsui and T. Agapie, Reduction Potentials of Heterometallic Manganese–Oxido Cubane Complexes Modulated by Redox-Inactive Metals, *Proc. Natl. Acad. Sci. U.S.A.*, 2013, **110**, 10084; (*b*) E. Y. Tsui, R. Tran, J. Yano and T. Agapie, Redox-Inactive Metals Modulate the Reduction Potential in Heterometallic Manganese–Oxido Clusters, *Nat. Chem.*, 2013, **5**, 293.

33 P. Pracht, F. Bohle and S. Grimme, Automated Exploration of the Low-Energy Chemical Space with Fast Quantum Chemical Methods, *Phys. Chem. Chem. Phys.*, 2020, **22**, 7169.

34 C. Bannwarth, S. Ehlert and S. Grimme, GFN2-xTB—An Accurate and Broadly Parametrized Self-Consistent Tight-Binding Quantum Chemical Method with Multipole Electrostatics and Density-Dependent Dispersion Contributions, *J. Chem. Theory Comput.*, 2019, **15**, 1652.

35 (*a*) A. D. Becke, Density-Functional Exchange-Energy Approximation with Correct Asymptotic Behavior, *Phys. Rev. A: At., Mol., Opt. Phys.*, 1988, **38**, 3098; (*b*) J. P. Perdew, Density-Functional Approximation for the Correlation Energy of the Inhomogeneous Electron Gas, *Phys. Rev. B: Condens. Matter Mater. Phys.*, 1986, **33**, 8822.

36 B. H. Solis and S. Hammes-Schiffer, Proton-Coupled Electron Transfer in Molecular Electrocatalysis: Theoretical Methods and Design Principles, *Inorg. Chem.*, 2014, **53**, 6427.

37 R. D. Shannon, Revised Effective Ionic Radii and Systematic Studies of Interatomic Distances in Halides and Chalcogenides, *Acta Crystallogr., Sect. A: Cryst. Phys., Diffr., Theor. Gen. Crystallogr.*, 1976, **32**, 751.

38 (*a*) S. Lin, C. S. Diercks, Y. B. Zhang, N. Kornienko, E. M. Nichols, Y. Zho, A. R. Paris, D. Kim, P. Yang, O. M. Yaghi and C. J. Chang, Covalent Organic Frameworks Comprising Cobalt Porphyrins for Catalytic $CO_2$ Reduction in Water, *Science*, 2015, **349**, 1208; (*b*) X.-M. Hu, M. H. Rønne, S. U. Pedersen, T. Skrydstrup and K. Daasbjerg, Enhanced Catalytic Activity of Cobalt Porphyrin in $CO_2$ Electroreduction upon Immobilization on Carbon Materials, *Angew. Chem., Int. Ed.*, 2017, **56**, 6468; (*c*) A. Call, M. Cibian, K. Yamamoto, T. Nakazono, K. Yamauchi and K. Sakai, Highly Efficient and Selective Photocatalytic $CO_2$ Reduction to CO in Water by a Cobalt Porphyrin Molecular Catalyst, *ACS Catal.*, 2019, **9**, 4867; (*d*) X. Zhang, M. Cibian, A. Call, K. Yamauchi and K. Sakai, Photochemical $CO_2$ Reduction Driven by Water-Soluble Copper(I) Photosensitizer with the Catalysis Accelerated by Multi-Electron Chargeable Cobalt Porphyrin, *ACS Catal.*,

2019, **9**, 11263; (*e*) J. L. Alvarez-Hernandez, A. A. Salamatian, J. H. Han and K. L. Bren, Potential- and Buffer-Dependent Selectivity for the Conversion of $CO_2$ to CO by a Cobalt Porphyrin-Peptide Electrocatalyst in Water, *ACS Catal.*, 2022, **12**, 14689.

39 (*a*) J.-M. Savéant and K. B. Su, Homogeneous Redox Catalysis of Electrochemical Reaction. Part VI, Zone Diagram Representation of the Kinetic Regimes, *J. Electroanal. Chem.*, 1984, **171**, 341; (*b*) C. Costentin and J.-M. M. Savéant, Multistep Molecular Catalysis of Electrochemical Reactions: Benchmarking of Homogeneous Catalysts, *ChemElectroChem*, 2014, **1**, 1226.